Journal of Molecular Structure 1062 (2014) 147–157

Contents lists available at ScienceDirect

Journal of Molecular Structure

journal homepage: www.elsevier.com/locate/molstruc

Mononuclear zinc(II) complexes of 2-((2-(piperazin-1-yl)ethylimino) methyl)-4-substituted phenols: Synthesis, structural characterization, DNA binding and cheminuclease activities

J. Ravichandran [a,b], P. Gurumoorthy [a], C. Karthick [a], A. Kalilur Rahiman [a,*]

[a] Post-Graduate and Research Department of Chemistry, The New College (Autonomous), Chennai 600 014, India
[b] Research and Development Department, Amrutanjan Healthcare Limited, Chennai 600 004, India

HIGHLIGHTS

- The molecular structure of complex was elucidated by single crystal XRD analysis.
- DNA binding studies support the intercalative mode of binding.
- Cleavage mechanism implies the involvement of hydroxyl radical as ROS.
- Complex containing the hydrophobic —CH_3 substituent shows higher DNA interactions.

GRAPHICAL ABSTRACT

Mononuclear zinc(II) complexes have been synthesized and characterized. X-ray crystal structure of complex **4** shows the distorted trigonal–bipyramidal geometry around the metal ion. Titration and voltammetry studies suggest the intercalation mode of binding with CT DNA. Oxidative cleavage of plasmid DNA proving the involvement of hydroxyl radical as ROS. DNA binding and cheminuclease activity exhibit a similar trend while expressing their potentials.

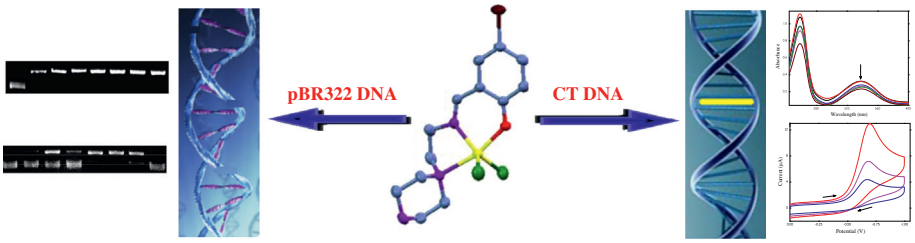

ARTICLE INFO

Article history:
Received 31 October 2013
Received in revised form 31 December 2013
Accepted 7 January 2014
Available online 23 January 2014

Keywords:
Schiff base
Zinc(II) complexes
Crystal structure
DNA binding
Cheminuclease activity

ABSTRACT

Four new zinc(II) complexes $[Zn(HL^{1-4})Cl_2]$ (**1–4**), where HL^{1-4} = 2-((2-(piperazin-1-yl)ethylimino)methyl)-4-substituted phenols, have been isolated and fully characterized using various spectro-analytical techniques. The X-ray crystal structure of complex **4** shows the distorted trigonal–bipyramidal coordination geometry around zinc(II) ion. The crystal packing is stabilized by intermolecular N—H···O hydrogen bonding interaction. The complexes display no d–d electronic band in the visible region due to d^{10} electronic configuration of zinc(II) ion. The electrochemical properties of the synthesized ligands and their complexes exhibit similar voltammogram at reduction potential due to electrochemically innocent Zn(II) ion, which evidenced that the electron transfer is due to the nature of the ligand. Binding interaction of complexes with calf thymus DNA was studied by UV–Vis absorption titration, viscometric titration and cyclic voltammetry. All complexes bind with CT DNA by intercalation, giving the binding affinity in the order of **2 > 1 ≫ 3 > 4**. The prominent cheminuclease activity of complexes on plasmid DNA (pBR322 DNA) was observed in the absence and presence of H_2O_2. Oxidative pathway reveals that the underlying mechanism involves hydroxyl radical.

1. Introduction

Past decades have evidenced an unprecedented progress in biological applications of inorganic drugs such as cisplatin,

* Corresponding author. Tel.: +91 44 2835 0297; fax: +91 44 2835 2883.
E-mail address: akrahmanjkr@gmail.com (A. Kalilur Rahiman).

http://dx.doi.org/10.1016/j.molstruc.2014.01.026
0022-2860/

carboplatin and oxaliplatin those serve as chemotherapeutic and diagnostic contrast agents [1,2]. However, they possess inherent limitations including intrinsic resistance and toxicity. So, the efforts to mitigate the drawbacks have prompted researcher to replace these platinum based drugs and, to develop the non-platinum based drugs with better efficacy. In this connection, transition metal complexes have shown enormous impact. The interaction of transition metal complexes with DNA has long been a subject of intensive investigation with the perspective development of newer materials for application in biotechnology and medicine. Generally, DNA is the primary intracellular target of anticancer drugs, so the molecules interact with DNA can cause DNA damage resulting in the death of cancer cell. These molecules can interact with DNA through the non-covalent modes such as groove binding, intercalation and external static electronic effects. Intercalation is the most important mode of binding. These investigations have resulted in the synthesis of many new transition metal based complexes, which bind to DNA through non-covalent interactions [3,4]. Cleavage of DNA may be considered as an enzymatic reaction which comprises various biological processes as well as the biotechnological manipulation of genetic material. In recent years, transition metal complexes have a massive impact on biological and industrial applications, because of its coordination behavior and importance in catalysis, either in bioinorganic or an organometallic chemistry [4–7]. Transition metal complexes with tunable coordination environments, versatile redox and spectral properties offer immense scope for designing species that are suitable to bind and cleave the DNA [8,9].

Zinc is one of the trace elements and second most abundant transition metal in several important biological processes. This element is an important one for the growth, development and differentiation of all types of life including microorganisms, plants and animals. The strong Lewis acidity, nucleophilic generation, leaving group stabilization, low toxicity, flexible coordination geometry, lack of redox property and 'borderline' hard–soft behavior make zinc as a suitable element for biological systems. Zinc hydrolases are enzymes that contain zinc(II) at the active site and that catalyze a variety of hydrolytic reactions involving many different substrates [10–12]. The chemistry of zinc compounds is gaining a great attention due to their interesting structural features, catechol oxidase, schizonticidal, antimalarial, antimicrobial, tumor photosensitizers and their potential as agricultural biocides [13–16]. Recent results of literature shows the efficacy of zinc(II) complexes in DNA binding and cleavage activities [17–19].

The foregoing facts stimulated our interest on the synthesis, structural characterization, DNA binding and cleavage activities of zinc(II) complexes containing the Schiff base ligand 2-((2-(piperazin-1-yl)ethylimino)methyl)-4-substituted phenol. In order to evaluate the changes in the interaction of Zn(II) complexes with DNA, different substituents are introduced in the Schiff base ligand. This may lead to changes in the electron density distribution around the transition metal complexes, which not only influence their spectral properties but renders a clear understanding in evaluating their interaction with DNA.

2. Experimental

2.1. Materials

The following chemicals were used for the synthesis of ligands and metal complexes. 5-Bromosalicylaldehyde, 5-chlorosalicylaldehyde and 1-(2-aminoethyl)piperazine were purchased from Sigma–Aldrich (USA). 5-Methylsalicylaldehyde was prepared according to the literature method [20]. Salicylaldehyde and the zinc(II) chloride were commercial products obtained from SD Fine (India) and these chemicals were used without further purification. Tetra(*n*-butyl)ammonium perchlorate (TBAP) used as the supporting electrolyte in the electrochemical measurements, was purchased from Fluka (Switzerland) and recrystallized from hot methanol (***Caution***: Perchlorate salts are potentially explosive while we have not experienced any problems with the compounds described, they should be treated with caution and handled in small quantities). Solvents were dried and purified before being used according to published procedure [21]. CT DNA and supercoiled pBR322 DNA were purchased from Bangalore Genei (India). 5 mM Tris–HCl/50 mM NaCl buffer solution was prepared from the combination of Tris base and NaCl dissolved in aqueous solution in which the pH was adjusted (till pH 7.2) with HCl/NaOH solution.

2.2. Physical methods

A micro-analysis (% C, H and N) was performed using Carlo Erba model 1106 elemental analyzer. ^{1}H and ^{13}C NMR spectral data were collected on VNMRS-400 spectrometer in $CDCl_3$ and DMSO (d_6) solution with tetramethylsilane (TMS) as an internal standard at ambient temperature. IR spectra were recorded using KBr pellets in the range 4000–400 cm^{-1} on a Bruker ALPHA FT-IR spectrometer. UV–Vis spectra of complexes were recorded in spectral grade DMF at 25 °C, on Agilent-8453 spectrophotometer in the range of 200–1100 nm, with a quartz cell and ε are expressed in $M^{-1}\,cm^{-1}$. ESI-mass spectra were recorded on a Q-Tof micromass spectrograph using H_2O as the mobile phase with an approximate concentration of 1.0 mmol dm^{-3}. The powder X-ray diffraction data of complexes **1**–**4** were collected on Rich Siefert 3000 diffractometer with graphite-monochromated Cu Kα_1 radiation (λ = 1.5406 Å). Cyclic voltammograms were obtained on CHI 602D (CH Instruments Co., USA) electrochemical analyzer. The measurements were carried out under oxygen free conditions using a three-electrode cell in which a glassy carbon was the working, a saturated Ag/AgCl was the reference and platinum wire was used as the auxiliary electrode. A ferrocene/ferrocenium (Fc/Fc^+) couple was used as an internal standard. The reported potentials are relative to the Ag/AgCl electrode and $E_{1/2}$ of the Fc/Fc^+ couple, which under the experimental conditions is 470 mV in DMF and ΔE_p for Fc/Fc^+ is 70 mV. Concentration of complexes was taken around 0.1 mM and TBAP was at 0.1 M.

2.3. Synthesis of ligands

All the ligands were prepared by the modified procedure of [1+1] Schiff base condensation reaction [22,23].

2.3.1. Synthesis of 2-((2-(piperazin-1-yl)ethylimino)methyl)phenol, HL^1

A methanolic solution (20 mL) of 1-(2-aminoethyl)piperazine (1.31 mL, 0.01 mol) was slowly added to a methanolic solution (20 mL) of salicylaldehyde (1.06 mL, 0.01 mol) with constant stirring. This reaction mixture was stirred for 2 h, and then refluxed for 4 h on water bath. Removal of solvent at reduced pressure gave the crude product as yellow oil. The product was washed twice with diethyl ether and recrystallized from chloroform. Yield: 1.65 g, 70.72%. Anal. Calc. for [$C_{13}H_{19}N_3O$], (FW: 233.31): C, 66.92; H, 8.21; N, 18.01. Found: C, 66.89%; H, 8.29%; N, 18.04%. IR (KBr, cm^{-1}): 3274 ν(—OH), 2948 ν(—NH), 1632 ν(C=N), 1371 ν(Ar—O). UV–Vis in methanol solution, λ_{max}/nm ($\varepsilon/M^{-1}\,cm^{-1}$): 245 and 316 (6270 and 1950, $\pi \rightarrow \pi^*$), 401 (825, $n \rightarrow \pi^*$). ^{1}H NMR (399.72 MHz, $CDCl_3$) δ/ppm: 13.42 (br s, 1H, phenolic proton), 8.35 (s, 1H, imine proton), 7.28 (m, 2H, Ar—H), 6.95 (d, J = 7.99 Hz, 1H, Ar—H), 6.87 (t, J = 7.19 Hz, 1H, Ar—H), 3.74 (t, J = 6.79 Hz, 2H, CH_2 protons), 2.89 (t, J = 4.40 Hz, 4H, CH_2 protons), 2.69 (t, J = 6.79 Hz, 2H, CH_2 protons), 2.51 (br s, 4H, CH_2 protons), 2.17

(br s, 1H, N—H proton). ^{13}C NMR (100.52 MHz, $CDCl_3$) δ/ppm: 165.6 (Ar—C=N), 161.2 (C—OH), 132.2, 131.2, 118.5 and 117.0 (aromatic carbons), 59.2, 56.8, 54.6 and 46.0 (CH_2 carbons). Mass EI *m/z*: 235.16 $[L^1+2H]^+$.

2.3.2. Synthesis of 2-((2-(piperazin-1-yl)ethylimino)methyl)-4-methylphenol, HL^2

The solid ligand HL^2 was prepared by following the procedure similar to that of HL^1 using 5-methylsalicylaldehyde instead of salicylaldehyde. Yield: 1.92 g, 77.63%. Color: Pale yellow. M.p.: 70.5 °C. Anal. Calc. for $[C_{14}H_{21}N_3O]$, (FW: 247.33): C, 67.98; H, 8.56; N, 16.99. Found: C, 67.96%; H, 8.63%; N, 17.02%. IR (KBr, cm^{-1}): 3275 ν(—OH), 2947 ν(—NH), 1637 ν(C=N), 1369 ν(Ar—O). UV–Vis in methanol solution, λ_{max}/nm (ε/M^{-1} cm^{-1}): 246 and 325 (6089 and 2354, $\pi \rightarrow \pi^*$), 413 (826, $n \rightarrow \pi^*$). ^{1}H NMR (399.72 MHz, $CDCl_3$) δ/ppm: 13.22 (br s, 1H, phenolic proton), 8.30 (s, 1H, imine proton), 7.11 (m, 1H, Ar—H), 7.03 (d, J = 1.60 Hz, 1H, Ar—H), 6.86 (d, J = 7.99 Hz, 1H, Ar—H), 3.73 (t, J = 6.39 Hz, 2H, CH_2 protons), 2.89 (t, J = 4.80 Hz, 4H, CH_2 protons), 2.68 (t, J = 7.19 Hz, 2H, CH_2 protons), 2.51 (br s, 4H, CH_2 protons), 2.28 (s, 3H, CH_3 protons), 1.97 (br s, 1H, N—H proton). ^{13}C NMR (100.52 MHz, $CDCl_3$) δ/ppm: 168.6 (Ar—C=N), 158.8 (C—OH), 133.0, 131.2, 127.5, 118.4 and 116.7 (aromatic carbons), 59.3, 56.9, 54.7 and 46.0 (CH_2 carbons), 20.3 (CH_3). Mass EI *m/z*: 249.02 $[L^2+2H]^+$.

2.3.3. Synthesis of 2-((2-(piperazin-1-yl)ethylimino)methyl)-4-chlorophenol, HL^3

The solid ligand HL^3 was prepared by following the procedure similar to that of HL^1 using 5-chlorosalicylaldehyde instead of salicylaldehyde. Yield: 1.96 g, 73.2%. Color: Yellow. M.p.: 69.5 °C. Anal. Calc. for $[C_{13}H_{18}N_3OCl]$, (FW: 267.76): C, 58.31; H, 6.77; N, 15.69. Found: C, 58.29%; H, 6.82%; N, 15.65%. IR (KBr, cm^{-1}): 3276 ν(—OH), 2947 ν(—NH), 1636 ν(C=N), 1360 ν(Ar—O). UV–Vis in methanol solution, λ_{max}/nm (ε/M^{-1} cm^{-1}): 244 and 326 (6117 and 1867, $\pi \rightarrow \pi^*$), 412 (874, $n \rightarrow \pi^*$). ^{1}H NMR (399.72 MHz, $CDCl_3$) δ/ppm: 13.24 (br s, 1H, phenolic proton), 8.28 (s, 1H, imine proton), 7.23 (m, 2H, Ar—H), 6.893 (d, J = 8.39 Hz, 1H, Ar—H), 3.74 (t, J = 6.99 Hz, 2H, CH_2 protons), 2.89 (t, J = 4.60 Hz, 4H, CH_2 protons), 2.68 (t, J = 6.79 Hz, 2H, CH_2 protons), 2.50 (br s, 4H, CH_2 protons), 2.05 (br s, 1H, N—H proton). ^{13}C NMR (100.52 MHz, $CDCl_3$) δ/ppm: 164.4 (Ar—C=N), 160.0 (C—OH), 132.0, 130.3, 123.0, 119.5 and 118.6 (aromatic carbons), 59.0, 56.6, 54.6 and 46.0 (CH_2 carbons). Mass EI *m/z*: 269.21 $[L^3+2H]^+$.

2.3.4. Synthesis of 2-((2-(piperazin-1-yl)ethylimino)methyl)-4-bromophenol, HL^4

The solid ligand HL^4 was prepared by following the procedure similar to that of HL^1 using 5-bromosalicylaldehyde instead of salicylaldehyde. Yield: 2.32 g, 74.30%. Color: Yellow. M.p.: 76 °C. Anal. Calc. for $[C_{13}H_{18}N_3OBr]$, (FW: 312.21): C, 50.01; H, 5.81; N, 13.46. Found: C, 50.03%; H, 5.86%; N, 13.43%. IR (KBr, cm^{-1}): 3275 ν(—OH), 2946 ν(—NH), 1634 ν(C=N), 1397 ν(Ar—O). UV–Vis in methanol solution, λ_{max}/nm (ε/M^{-1} cm^{-1}): 251 and 328 (6390 and 1882, $\pi \rightarrow \pi^*$), 414 (1273, $n \rightarrow \pi^*$). ^{1}H NMR (399.72 MHz, $CDCl_3$) δ/ppm: 13.29 (br s, 1H, phenolic proton), 8.28 (s, 1H, imine proton), 7.36 (d, J = 2.59 Hz, 2H, Ar—H), 6.85 (d, J = 8.79 Hz, 1H, Ar—H), 3.74 (t, J = 6.99 Hz, 2H, CH_2 protons), 2.89 (t, J = 4.80 Hz, 4H, CH_2 protons), 2.68 (t, J = 2.99 Hz, 2H, CH_2 protons), 2.50 (br s, 4H, CH_2 protons), 1.79 (br s, 1H, N—H proton). ^{13}C NMR (100.52 MHz, $CDCl_3$) δ/ppm: 164.3 (Ar—C=N), 160.4 (C—OH), 134.8, 133.3, 120.1, 119.1 and 109.8 (aromatic carbons), 59.0, 56.6, 54.6 and 46.0 (CH_2 carbons). Mass EI *m/z*: 313.76 $[L^4+2H]^+$.

2.4. General procedure for synthesis of metal complexes

All complexes were synthesized using the same procedure as given below: A methanolic solution (20 mL) of $ZnCl_2$ (0.54 g, 0.004 mol) was added slowly to an equimolar amount of appropriate ligand (HL^{1-4}, 0.004 mol) in methanol (20 mL) with constant stirring. This mixture was stirred for 2 h, and the reaction was carried out for 6 h under reflux. After cooling the reaction mixture to room temperature, the resulting product was washed with diethyl ether and dried in *vacuo*. Effort was taken to get single crystal, complex **4** only gave crystals of good diffraction quality and other complexes went unsuccessful.

2.4.1. $[Zn(HL^1)Cl_2]$, **1**

Yield: 1.13 g, 76.4%. Color: Yellow. Anal. Calc. for $[C_{13}H_{19}N_3OCl_2Zn]$, (FW: 369.59): C, 42.24; H, 5.18; N, 11.37. Found: C, 42.29%; H, 5.28%; N, 11.43%. IR (KBr, cm^{-1}): 3499 ν(—OH str. of CH_3OH), 2985 ν(N—H str. of $>NH_2^+$), 1621 ν(C=N), 1599 ν(N—H bend. of NH_2^+) 1355 ν(Ar—O). UV–Vis in DMF solution, λ_{max}/nm (ε/M^{-1} cm^{-1}): 255 (5778, $\pi \rightarrow \pi^*$), 328 (1719, $n \rightarrow \pi^*$). ESI-MS (H_2O) display peaks at: $[ZnL^1+2H]^{2+}$ (302), $[ZnL^1]^+$ (299), $[L^1+H]$ (234).

2.4.2. $[Zn(HL^2)Cl_2]$, **2**

Yield: 1.26 g, 82.3%. Color: Yellow. Anal. Calc. for $[C_{14}H_{21}N_3OCl_2Zn]$, (FW: 383.62): C, 43.83; H, 5.52; N, 10.95. Found: C, 43.86%; H, 5.59%; N, 10.98%. IR (KBr, cm^{-1}): 3489 ν(—OH str. of CH_3OH), 2983 ν(N—H str. of $>NH_2^+$), 1629 ν(C=N), 1597 ν(N—H bend. of NH_2^+), 1354 ν(Ar—O). UV–Vis in DMF solution, λ_{max}/nm (ε/M^{-1} cm^{-1}): 259 (6361, $\pi \rightarrow \pi^*$), 338 (1882, $n \rightarrow \pi^*$). ESI-MS (H_2O) display peaks at: $[ZnL^2+H]^{2+}$ (314), $[ZnL^2]^+$ (313), $[L^2+H]$ (248).

2.4.3. $[Zn(HL^3)Cl_2]$, **3**

Yield: 1.32 g, 81.9%. Color: Yellow. Anal. Calc. for $[C_{13}H_{18}N_3OCl_3Zn]$, (FW: 404.04): C, 38.64; H, 4.49; N, 10.4. Found: C, 38.67%; H, 4.62%; N, 10.48%. IR (KBr, cm^{-1}): 3447 ν(—OH str. of CH_3OH), 2981 ν(N—H str. of $>NH_2^+$), 1627 ν(C=N), 1576 ν(N—H bend. of NH_2^+), 1348 ν(Ar—O). UV–Vis in DMF solution, λ_{max}/nm (ε/M^{-1} cm^{-1}): 269 (7386, $\pi \rightarrow \pi^*$), 382 (6953, $n \rightarrow \pi^*$). ESI-MS (H_2O) display peaks at: $[ZnL^3+H]^{2+}$ (334), $[L^3+2H]^+$ (270), $[L^3+H]$ (268).

2.4.4. $[Zn(HL^4)Cl_2]$, **4**

Yield: 1.84 g, 83.1%. Color: Yellow. Anal. Calc. for $[C_{13}H_{18}N_3OBrCl_2Zn]$, (FW: 448.49): C, 34.81; H, 4.04; N, 9.37. Found: C, 34.86%; H, 4.13%; N, 9.42%. IR (KBr, cm^{-1}): 3441 ν(—OH str. of CH_3OH), 2979 ν(N—H str. of $>NH_2^+$), 1622 ν(C=N), 1586 ν(N—H bend. of NH_2^+), 1383 ν(Ar—O). UV–Vis in DMF solution, λ_{max}/nm (ε/M^{-1} cm^{-1}): 268 (6235, $\pi \rightarrow \pi^*$), 382 (5133, $n \rightarrow \pi^*$). ESI-MS (H_2O) display peaks at: $[ZnL^4]^{2+}$ (375), $[L^4+2H]^+$ (314), $[L^4+H]$ (312).

2.5. Single crystal X-ray diffraction experiments

Single crystals suitable for X-ray diffraction measurements were obtained by the slow evaporation of complex **4** in methanol/DMF at room temperature. A pale yellow crystals obtained was sorted using polarizing microscope (Leica DMLSP). Crystals having good morphology were chosen for three-dimensional intensity data collection. A crystal with dimensions of 0.20 × 0.15 × 0.10 mm was mounted on a glass fiber for diffraction experiment. X-ray single crystal data were collected on a 'Kappa Apex2 CCD diffractometer' equipped with a fine-focus sealed tube X-ray source and graphite monochromated Mo ($K\alpha$) radiation in the wavelength (λ) of 0.71073 Å at room temperature (293 ± 2 K). The intensity data were collected using ω and φ scans with frame width of 0.5°. The frame integration and data reduction were performed using 'Bruker SAINT-plus' (Version 7.06a) software. Empir-

ical absorption corrections were applied for complex, using 'SADABS' program [24]. The structure was solved by using 'SIR92' [25] and the full-matrix least-squares refinement on F^2 was performed using 'SHELXL-97' program [26]. After several cycles of refinement, the positions of the hydrogen atoms were calculated and added to the refinement process. Molecular graphics, hydrogen bonding and packing figures were generated by using the softwares 'ORTEP 3.0' [27] and 'Mercury 3.0' [28]. The final *R*-value of complex **4** was 0.0350, and the final electrodensity map contains maximum and minimum peak heights of 0.954 and −0.729 e $Å^{-3}$, respectively.

2.6. DNA binding studies

2.6.1. Absorption spectral titration

The application of electronic absorption spectra in DNA interaction is one of the most effective method to examine the binding mode and strength of metal complexes with DNA. A solution of calf thymus DNA in the Tris–HCl/NaCl buffer gave a ratio of UV absorbance at 260 and 280 nm of about 1.85:1, indicating that the DNA was sufficiently free from proteins [29].

Stock solutions of CT DNA was prepared in Tris–HCl/NaCl buffer and stored at 4 °C for less than 4 days. The DNA concentration per nucleotide was determined by absorption spectroscopy using the molar absorption coefficient 6600 M^{-1} cm^{-1} at 260 nm [30]. Stock solution of metal complexes was prepared by using 5% DMF/Tris–HCl (0.5 mL DMF in 10 mL buffer) and diluting suitably with the corresponding buffer to the required concentration for all the experiments. Absorption titration experiments were carried out by varying the nucleic acid concentration (0–250 μM) and maintaining complex concentration constant (30 μM). Complex-DNA solutions were allowed to incubate for 30 min at room temperature before measurements were taken. While measuring the absorption spectra, equal amounts of DNA was added to both complex solution and the reference solution to eliminate the absorbance of DNA itself at the measured wavelength. Absorbances were recorded after each successive addition of DNA solution and equilibration (i.e., when there was no further change) at room temperature.

Titration curves were constructed from the fractional change in the absorption intensity as a function of DNA concentration [31,32]. The intrinsic binding constant K_b, can be obtained by the following equation:

$$[DNA]/(\varepsilon_a - \varepsilon_f) = [DNA]/(\varepsilon_b - \varepsilon_f) + 1/K_b(\varepsilon_b - \varepsilon_f)$$

where [DNA] is the DNA concentration in M (nucleotide), ε_a is the absorption coefficient observed at a given DNA concentration, ε_f is the absorption coefficient of complex in the absence of DNA, ε_b is the absorption coefficient of complex when fully bound to DNA, and K_b is the intrinsic binding constant in M^{-1}.

Each set of data were fitted to the above equation, and the plot of $[DNA]/(\varepsilon_a - \varepsilon_f)$ *versus* [DNA] gave a slope and the *y*-intercept which are equal to $1/(\varepsilon_b - \varepsilon_f)$ and $1/K_b(\varepsilon_b - \varepsilon_f)$, respectively. The intrinsic binding constant K_b was obtained from the ratio of the slope to the intercept.

2.6.2. Hydrodynamic (Viscosity) measurements

Viscometric titrations were conducted on an Ostwald micro viscometer of 2 mL capacity, immersed in a water bath maintained at 25 ± 0.1 °C. The desired concentrations of DNA (200 μM) and complexes (10–100 μM) were prepared by using Tris–HCl/NaCl buffer. Mixing of the solution was achieved by purging the nitrogen gas through viscometer. The flow time was measured with a digital stopwatch and, the experiment was repeated in triplicate to get the concurrent values. Data were presented as $(\eta/\eta_0)^{1/3}$ *versus* binding ratio (1/*R*) [complex]/[DNA] [33,34], where η and η_0 are the specific viscosity of DNA in the presence and absence of complex, respectively. The values of η and η_0 were calculated from the relation [35]:

$$\eta = (t - t_b)/t_b$$

where t_b is the flow time of buffer alone and, t is the observed flow time for DNA in the absence and presence of complex. Relative viscosities for DNA were obtained from the relation, η/η_0.

2.6.3. Electrochemical titration

Electrochemical techniques are best complementary to other related biophysical techniques that are applied to study the interaction between redox active molecules and biomolecules [36]. Double distilled water was used to prepare the buffer solutions. The solutions of complexes and DNA were prepared by using DMF and Tris–HCl/NaCl buffer (pH 7.2), respectively. The concentration of complexes can be taken as 0.1 mM and 100, 200 μM for DNA. Solutions were deaerated by purging with N_2 gas for 10 min prior to measurements.

2.7. Cheminuclease activity

Cheminuclease activity of complexes **1**–**4**, on plasmid DNA (pBR322 DNA) was monitored by using the agarose gel electrophoresis technique. The DNA cleavage efficiency was monitored by determining their ability to convert supercoiled DNA (Form I) to open circular (Form II) and linear forms (Form III). In cleavage reactions, supercoiled pBR322 plasmid DNA (33.3 μM) was treated with zinc(II) complexes in Tris–HCl/NaCl buffer. In each experiment, plasmid DNA was treated with different concentration of complexes (50–500 μM), H_2O_2 (40 μM, oxidizing agent), DMSO (0.2 mM, hydroxyl radical scavenger), and was monitored using gel electrophoresis. The samples were incubated for 1 h at 37 °C. A loading buffer containing 0.25% bromophenol blue, 0.25% xylene cyanol, 30% glycerol (3 μL) was added and the electrophoresis of the DNA cleavage products were performed on 0.8% agarose gel containing ethidium bromide (1 μg/mL). The gels were run at 50 V for 1 h in TAE buffer (40 mM Tris base, 20 mM acetic acid, 1 mM EDTA, pH 8.3). The bands were viewed by placing the gel on UV illuminator and were photographed.

3. Results and discussion

3.1. Synthesis and spectral characterization

The synthesized Schiff base ligands HL^{1-4} and their zinc(II) complexes **1**–**4** have been isolated by using general procedure and obtained in good yield (Scheme 1). They are non-hygroscopic in nature. The yellowish ligands are soluble in most of the organic solvents and complexes are soluble in water, Tris–HCl/NaCl buffer, DMF and DMSO. The authenticities of ligands were ascertained by elemental analysis, IR, NMR and mass spectroscopy. The stoichiometries of complexes were determined based on elemental analysis and spectral methods. The mass spectra of ligands and complexes showed the primary peaks of the expected products. ESI-MS spectra shows the corresponding peaks and suggesting the proposed formulae of complexes, and it was confirmed by single crystal X-ray diffraction technique of complex **4**.

The IR spectra of ligands and their complexes shows broad O—H stretching band due to an intramolecular hydrogen bonding (O—H···N). In complexes **1**–**4**, coordination of azomethine nitrogen was supported by shifting of ν(C=N) to lower frequency (9–12 cm^{-1}) as compared to those of free ligands [37,38]. Upon complexation, ν(Ar—O) stretching is also shifted to lower frequency, suggesting coordination *via* the phenoxide atom, and further confirmed by X-ray crystal structure of **4**. The band observed around

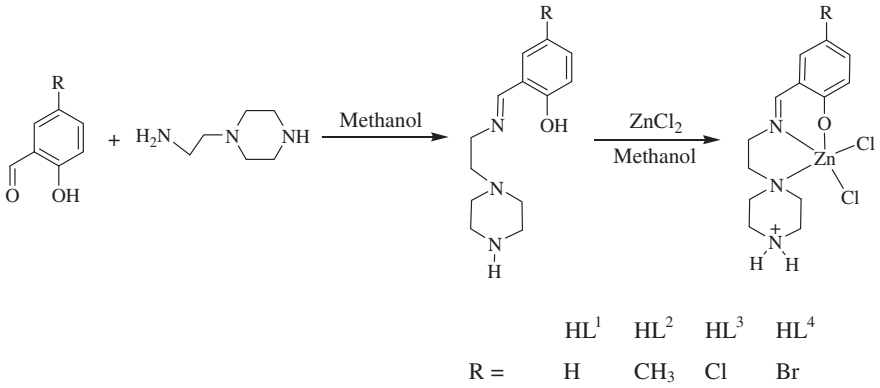

Scheme 1. Schematic route for synthesis of ligands (HL^{1-4}) and complexes (**1**–**4**).

2947 cm^{-1} is assigned to N—H stretching of secondary amine of ligands and, the complexes exhibits a medium intensity bands in the region of 2985–2979 cm^{-1} and 1599–1576 cm^{-1} due to N—H stretching and bending of piperazinium ion [39], respectively. Hydrogen and carbon resonance spectra (Fig. S1 and S2) were recorded at 298 K. In the ^1H NMR spectra, the methylene hydrogen atoms adjacent to the imine bond shows triplet at δ 3.74, and the same resonance observed for complexes with a significant downfield shift, clearly indicates the coordination of imine nitrogen with the metal. The azomethine resonance in complexes showed a downfield shift (~0.3 δ) compared to those of free ligands, revealing deshielding of azomethine group due to coordination with the metal ion. Absorption spectra of ligands and complexes (**1**–**4**) exhibits charge transfer transitions in the region of 244–414 and 255–382 nm, respectively. The absence of band above 400 nm is due to the lack of metal to ligand charge transfer transition, because of d^{10} electronic configuration of zinc(II) complexes. Cyclic voltammograms of ligands (Fig. S3) and complexes show one electron irreversible reduction wave which may be due to an electron transfer of imine group or phenoxide atom, since zinc(II) ion is an electrochemically innocent. The less negative reduction potential observed for complexes of ligands $L^{3\&4}$ when compared to other complexes of ligands $L^{1\&2}$ is due to presence of the electron withdrawing substituent. i.e., the complexes containing electron withdrawing substituent at the para position to phenoxide ion in the phenyl ring is reduced at less negative potential, which decreases the electron density around complex and favors easy reduction [40].

3.2. Crystal structure

The complex **4** crystallizes as **4**·CH_3OH·DMF in monoclinic system with space group *C*2/*c*, *Z* = 8 (*a* = 28.0094(9), *b* = 11.6668(3), *c* = 15.3766(5) Å). The methanol and dimethylformamide molecules found in the crystal are not coordinated to zinc(II) ion and occupies the crystal lattice as free molecules. The single crystal structure of **4**·CH_3OH·DMF has been solved and the crystal data and structure refinement details are given in Table 1. The ORTEP diagram is given in Fig. 1, while the selected bond lengths and angles are given in Table 2. The zinc(II) ion in the complex is five coordinated and the geometry around the zinc nuclei is best described as a distorted trigonal–bipyramidal with a large contribution from the trigonal–bipyramidal distortion constant (or) structural index parameter (τ) 0.657 ($\tau = (\beta - \alpha)/60$ where β and α (in °) are the two largest L–M–L angles O(1)—Zn(1)—N(2) = 164.63(10)° andN(1)—Zn(1)—Cl(2) = 125.17(9)°, a regular trigonal-bipyramid (TBP) and square-based pyramid (SP) have τ values of 1 and 0, respectively [41–43]). The five coordination sites of zinc(II) metal center can be described as below: An imine (N1) and piperazine (N2) nitrogen atoms, and one phenolate oxygen (O1) atom were coordinated in an equatorial plane to the zinc(II) ion at a distance of Zn(1)—N(1) = 2.055(3) Å, Zn(1)—N(2) = 2.359(3) Å and Zn(1)—O(1) = 2.062(2) Å, respectively. The fourth and fifth coordination positions of the Zn(1) atom is occupied by two chloride ions with distance of 2.2807(10) and 2.2764(11) Å, respectively for Zn(1)—Cl(1) and Zn(1)—Cl(2), with an Cl(1)—Zn(1)—Cl(2) angle of 116.36(4)°.

Table 1
Crystal data and structure refinement for complex **4**·CH_3OH·DMF.

CCDC	904783
Empirical formula	$C_{17}H_{29}BrCl_2N_4O_3Zn$
Formula weight	553.62
Temperature (K)	293 ± 2
Wavelength (Å)	0.71073
Crystal system	Monoclinic
Space group	*C*2/*c*
a (Å)	28.0094(9)
b (Å)	11.6668(3)
c (Å)	15.3766(5)
α (°)	90
β (°)	109.9770(10)
γ (°)	90
Volume (Å^3)	4722.4(2)
Z	8
Calculated density (Mg/m^3)	1.557
Absorption coefficient (mm^{-1})	2.982
F(000)	2256
Crystal size (mm)	0.20 × 0.15 × 0.10
θ range for data collection (°)	2.71–25.00
Limiting indices	$-33 \leqslant h \leqslant 33$, $-11 \leqslant k \leqslant 13$, $-17 \leqslant l \leqslant 18$
Reflections collected	20395
Independent reflections	4159 [*R*(int) = 0.0302]
Max. and min. transmission	0.7547 and 0.6669
Refinement method	Full-matrix least-squares on F^2
Data/restrains/parameters	4159/74/317
GOF on F^2	1.039
Final *R* indices [$I > 2\sigma(I)$]	R_1 = 0.0350, wR_2 = 0.0855
R indices (all data)	R_1 = 0.0509, wR_2 = 0.0952
Largest diff. peak and hole (e Å^{-3})	0.954 and −0.729

Non-covalent interactions like π-stacking interactions with aryl hydrogen and hydrogen bonding network plays a vital role in supramolecular chemistry and crystal engineering [44]. The hydrogen bonding parameters are listed in Table 3. The molecular packing (Fig. S4) and hydrogen bonding (Fig. 2) diagrams reveals that the complex molecules are interconnected through intermolecular N—H···O hydrogen bonds formed between nitrogen atom (N3) of the piperazine and oxygen atoms of the phenolate group (O1) and DMF (O2) solvent molecule of adjacent complex unit,

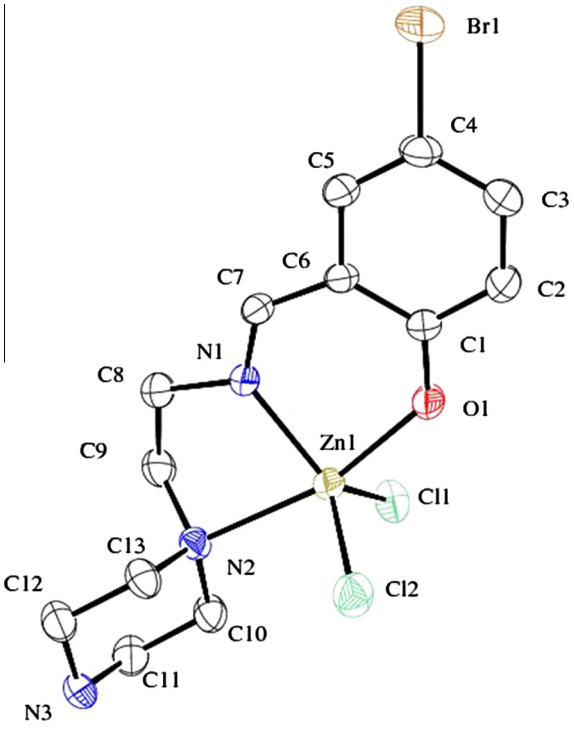

Fig. 1. ORTEP representation of complex **4**·CH_3OH·DMF showing atom numbering scheme and displacement ellipsoid (30% probability level). (Hydrogen atoms, lattice methanol and N,N-dimethylformamide molecules are omitted for clarity).

Table 2
Selected bond lengths (Å) and bond angles (°).

Bond lengths (Å)			
Zn(1)—N(1)	2.055(3)	Zn(1)—Cl(1)	2.2807(10)
Zn(1)—N(2)	2.359(3)	Zn(1)—Cl(2)	2.2764(11)
Zn(1)—O(1)	2.062(2)		
Bond angles (°)			
N(1)—Zn(1)—O(1)	87.27(10)	Cl(1)—Zn(1)—Cl(2)	116.36(4)
N(1)—Zn(1)—Cl(2)	125.17(9)	N(1)—Zn(1)—N(2)	77.41(10)
O(1)—Zn(1)—Cl(2)	95.63(9)	O(1)—Zn(1)—N(2)	164.63(10)
N(1)—Zn(1)—Cl(1)	118.15(9)	Cl(2)—Zn(1)—N(2)	92.21(8)
O(1)—Zn(1)—Cl(1)	92.85(9)	Cl(1)—Zn(1)—N(2)	95.49(7)

Table 3
Hydrogen bonds for complex **4**·CH_3OH·DMF [Å and °].

D—H···A	d(D—H)	d(H···A)	d(D···A)	∟(DHA)
N(3)—H(3A)···O(2)#2	0.889(18)	1.91(2)	2.784(10)	169(3)
N(3)—H(3B)···O(1)#3	0.902(19)	1.80(2)	2.694(4)	169(4)

Symmetry transformations used to generate equivalent atoms: #1 $-x+1, y, -z+3/2$; #2 $x, y+1, z$; #3 $x, -y+1, z-1/2$.

respectively [N(3)—H(3B)···O(1) = 2.694(4), N(3)—H(3A)···O(2) = 2.784(10)].

In addition to the single crystal X-ray studies of complex **4**, in order to test the degree of crystallinity of other complexes, we obtained the powder XRD pattern of all complexes **1**–**4**. The powder X-ray diffraction analysis is used to determine the phase identification of unknown crystalline materials, purity and particle size of the compounds. The powder XRD analysis of complexes was recorded in the (2θ) 10–70° range and diffractograms are given in Fig. S5, which shows well resolved sharp peaks with high intensities. The XRD patterns indicate crystalline nature of the complexes. The observed large number of feeble peaks imply uniform phase with no impurity present in the complexes [45].

3.3. DNA binding properties

3.3.1. Stability of complexes in buffer

DNA interactions have been performed in Tris–HCl/NaCl buffer, so it was necessary to check the stability of complexes (**1**–**4**) in this buffer. A negligible absorbance and current change was observed after 96 h in electronic spectra and cyclic voltammetry, respectively. Little absorbance/current change without any considerable shift in wavelength/potential predicted the stability of complexes in this buffer.

3.3.2. Absorption spectral titration

The binding mode and strength of complexes to CT DNA have been usually studied by various spectroscopic techniques. Monitoring the effect of increasing amounts of DNA on the absorption spectrum of a drug is one of the most widely used methods for determining overall binding constants. Transition metal complexes can bind to DNA *via* both covalent and/or non-covalent interactions. In the case of covalent binding, the labile ligand of the complex can be replaced by a nitrogen base of DNA such as guanine (N7), while the non-covalent interactions include intercalative, electrostatic and groove (surface) binding of metal complexes outside of DNA helix, along major/minor groove. In general, an intercalative binding mode of molecule to DNA is accompanied by hypochromism and/or significant red (bathochromism) or blue (hypsochromism) shift due to the strong π–π stacking interaction between the DNA base pairs and aromatic chromophore of ligand with the extent of hypochromism and red shift commonly consistent with the strength of the intercalation [46].

The absorption spectra of complexes **1** and **2** in the absence and presence of CT DNA are given in Figs. 3 and 4 (absorption spectra obtained for complexes **3** and **4** are shown in Figs. S6 and S7). The absorption spectral properties of complexes **1**–**4** bound to CT DNA is shown in Table 4. With increasing concentration of DNA, the absorption bands of complexes were affected, resulting in the tendency of hypochromism and a slight red shift. The observed hypochromism (red shift, nm) of 18% (3), 32% (2.5), 8% (1) and 4% (1) for complexes **1**–**4**, respectively, at a ratio (R) of [DNA]/[complex] = 10, unambiguously reveal the intercalative binding mode of complexes with CT DNA [47,48]. Hypochromism and bathochromism suggest the stacking interaction between an aromatic ring of the ligand and the base pairs of DNA. After interaction of complex with the base pairs of DNA, the π^* orbital of intercalated ligand can couple with the π orbitals of base pairs, thus decreasing the π–π^* transition energy, hence resulting in hypochromism [49].

The decrease in order of hypochromism reflects the decrease in DNA binding affinities of complexes in the same order. To enable quantitative comparison of DNA binding affinities, the intrinsic binding constants, K_b of complexes **1**–**4** are calculated as 6.0 ($\pm$0.7) $\times 10^4\ M^{-1}$, 7.9 ($\pm$1.3) $\times 10^4\ M^{-1}$, 2.7 ($\pm$0.9) $\times 10^4\ M^{-1}$ and 1.8 ($\pm$0.7) $\times 10^4\ M^{-1}$, respectively. The binding strength of complexes are lower than that of the reported classical intercalators (EtBr, in Tris–HCl/NaCl buffer (25:40), pH 7.9 and $[Ru(phen)_2(dppz)]^{2+}$), in which the binding constants have been found to be in the order of 10^6–$10^7\ M^{-1}$ [50]. Additionally, hydrogen bonding is also possible in the interaction of DNA with complexes. DNA possesses several hydrogen bonding sites in major as well as minor grooves, and complexes **1**–**4** contain —NH groups, there could be hydrogen bonding between the complexes and the base pairs in DNA [30]. However, the hydrogen bonding is a weak interaction. Hence from the obtained results, it has been found that complexes **2** and **1** exhibit better binding affinity with CT DNA than the other

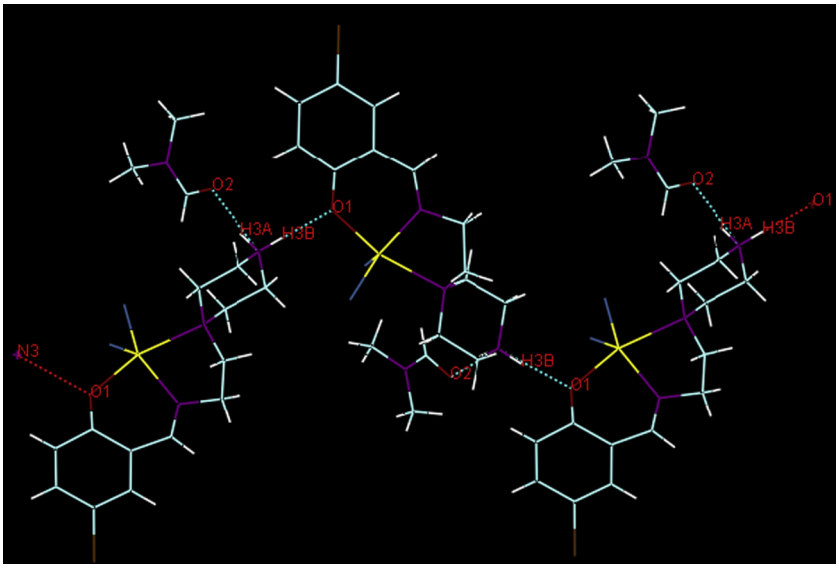

Fig. 2. Hydrogen bonding of complex **4**·CH_3OH·DMF.

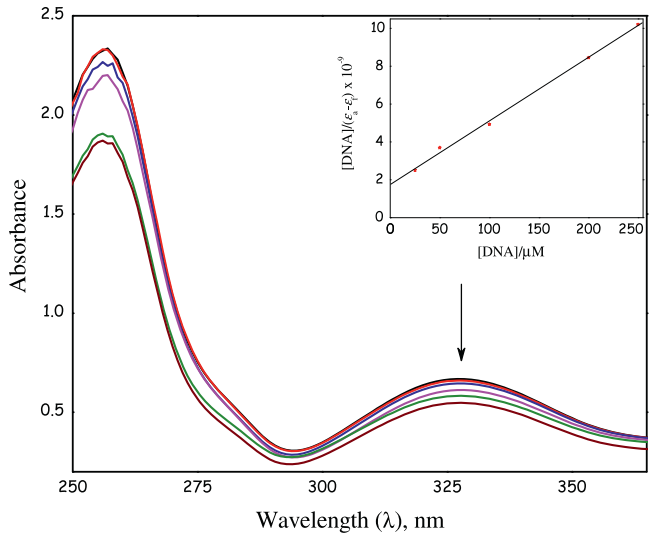

Fig. 3. Absorption spectra of complex **1** (30 μM) in Tris–HCl/NaCl (pH 7.2) buffer upon addition of CT DNA (0–250 μM) . Arrow shows the absorption decreases upon increasing concentration of DNA. Inset: Plot of $[DNA]/(\varepsilon_b - \varepsilon_f)$ *versus* [DNA] for absorption titration of CT DNA with complex.

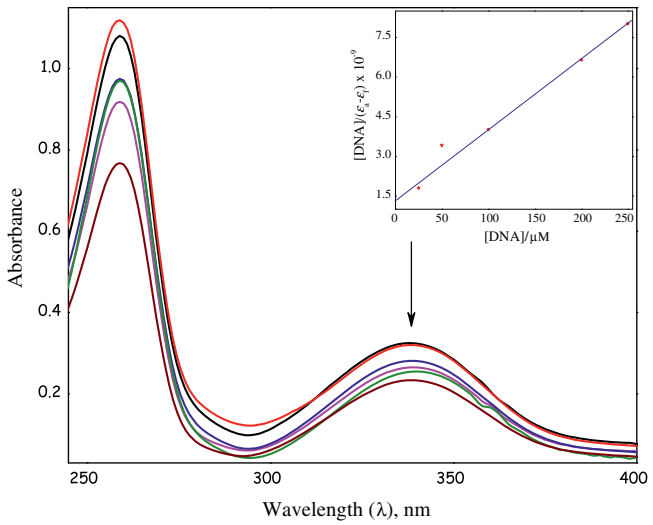

Fig. 4. Absorption spectra of complex **2** (30 μM) in Tris–HCl/NaCl (pH 7.2) buffer upon addition of CT DNA (0–250 μM) . Arrow shows the absorption decreases upon increasing concentration of DNA. Inset: Plot of $[DNA]/(\varepsilon_b - \varepsilon_f)$ *versus* [DNA] for absorption titration of CT DNA with complex.

complexes and, the binding strength of complexes decreases in the order of **2 > 1** ≫ **3 > 4**. The higher hypochromism and K_b value obtained for complex **2** suggest its higher binding affinity to DNA than that for other complexes. This may be due to the presence of methyl group on phenyl ring which is involved in hydrophobic interaction with the hydrophobic DNA surface that leads to enhancement of DNA binding affinity. The observed less binding affinity of complex **4** may be due to the presence of comparatively larger size of the Br atom on the phenyl ring when compared to Cl present in complex **3**, which disturb the intercalation of DNA base pairs.

3.3.3. Hydrodynamic (Viscosity) measurements

The viscosity measurement plays a pivotal role in the investigation of binding mode of complexes with DNA. To apprehend the nature of DNA binding of complexes, we carried out viscosity measurements on CT DNA by varying the concentration of added complexes. The values of relative specific viscosity (η/η_0), where η and η_0 are the specific viscosities of DNA in the presence and absence of complex, are plotted against $1/R$ ([Complex]/[DNA] = 0.05–0.5). In classical intercalation, the DNA helix lengthens as base pairs are separated to accommodate the binding ligand leading to the increase in DNA viscosity, whereas a partial, non-classical intercalation of ligand cause a bend (or kink) in DNA helix reducing its effective length and thereby its viscosity. Therefore, viscosity measurements, which is sensitive to the changes in the length of DNA molecule, is regarded as the least ambiguous and most critical means of studying the binding mode of metal complexes with DNA in solution and provide stronger arguments for an intercalation binding mode [35,51].

The effect of complexes **1**–**4** on the viscosity of DNA is shown in Fig. 5. Ethidium bromide has been well-known to bind to DNA in an intercalation mode and increases the relative viscosity for the lengthening of DNA helix. The relative viscosity of DNA is steadily

Table 4
Absorption spectral properties of complexes **1**–**4** bound to CT DNA.

Complex	λ (nm)	R	Change in absorption	$\Delta\lambda$ (nm)	[a]H%	K_b (10^4 M^{-1})
1	328	10	Hypochromism	3	18	6.0 ± 0.7
2	338	10	Hypochromism	2.5	32	7.9 ± 1.3
3	386	10	Hypochromism	1	8	2.7 ± 0.9
4	385	10	Hypochromism	1	4	1.8 ± 0.7

Measurements were made at R = 10, where R = [DNA]/[complex]; [DNA] = 0–250 μM; [Complex] = 30 μM.
[a] $H\% = [(A_{free} - A_{bound})/A_{free}] \times 100\%$.

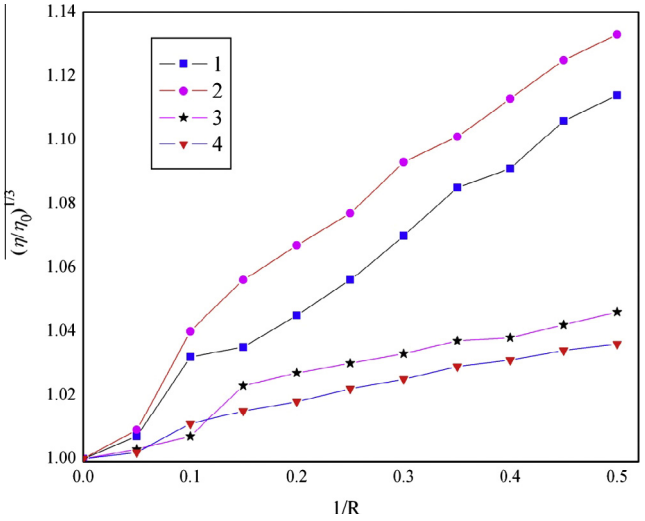

Fig. 5. Effect of complexes **1**–**4** on the viscosity of CT DNA. Relative specific viscosity *versus* 1/R (R = [DNA]/[Complex], [DNA] = 200 μM, [Complex] = 10–100 μM).

increased upon increasing amount of complexes **1**–**4**, similar to the behavior of EtBr. These results suggest that complexes **1**–**4** can intercalate between the base pairs of DNA. The binding ability of complexes to increase the viscosity of DNA varies in the order **2** > **1** > **3** > **4**, which parallels the hypochromism and DNA binding affinities. Thus, the complexes show an increase in viscosity, which is lower than that for the classical intercalator ethidium bromide [52]. The highest increase in DNA viscosity was effected by **2**, suggesting that this complex dramatically increase the hydrodynamic length of DNA as a consequence of the untwisting of the base pairs and helical backbone of DNA needed to accommodate the intercalators [53].

3.3.4. Electrochemical titration

Cyclic voltammetry is a supporting tool in DNA interaction with redox active molecules and may yield information about the interaction mode with both oxidized and reduced form of the metal ion. In general, when the metal complex binds to DNA *via* intercalation, the potential presents a positive shift, while in the case of electrostatic interaction, the potential will shift to a negative direction. If more than one potential exist simultaneously, a positive and negative shift of E_p^1 and E_p^2, respectively, the molecule can bind to DNA by both intercalation and electrostatic interaction [31].

Electrochemical parameters of each complex in the absence and presence of CT DNA are given in Table 5. On the incremental addition of CT DNA (R = [DNA]/[complex]) to the metal complexes, no new reduction waves (Fig. 6) appeared and the observed decrease in current intensity (*i.e.,* the values of i_{pc} and E_{pc}) attributed to the diffusion of an equilibrium mixture of free and DNA-bound complex to the electrode surface and suggest the existence of the same electrochemical behavior upon addition of CT DNA. Thus, the

Table 5
Electrochemical parameters for complexes **1**–**4** in the absence and presence of CT DNA.

Complexes	R	i_{pc} (10^{-5} A)	E_{pc} (V)
1	0	1.45	−0.692
	1	1.05	−0.686
	2	0.95	−0.684
2	0	1.30	−0.697
	1	0.75	−0.684
	2	0.44	−0.673
3	0	1.30	−0.663
	1	1.10	−0.652
	2	0.90	−0.649
4	0	0.85	−0.665
	1	0.75	−0.649
	2	0.70	−0.644

CV measured at 100 mV^{-1}. E (V) vs. Ag/AgCl conditions: GC working, Pt wire counter and Ag/AgCl reference electrodes; R = [DNA]/[complex]; [DNA] = 100 and 200 μM; [complex] = 100 μM; Supporting electrolyte [TBAP] = 0.1 M.

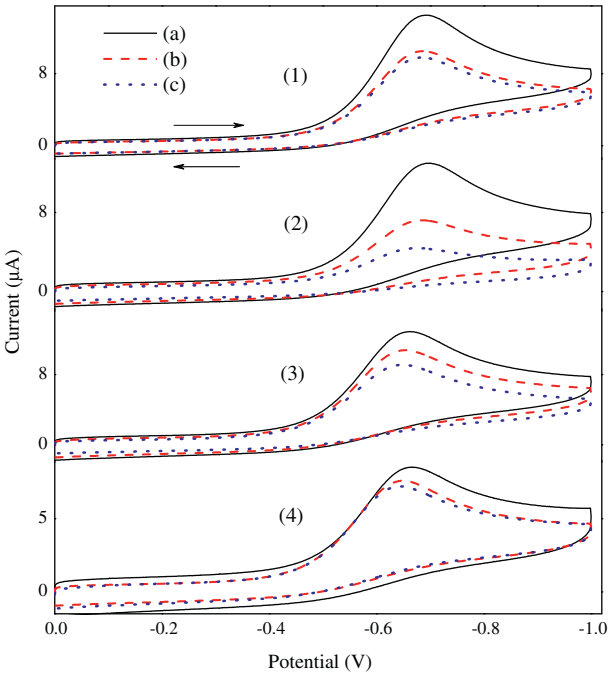

Fig. 6. Cyclic voltammograms of complexes **1**–**4** in the absence (a) and presence of CT DNA. [Complex] = 100 μM, [DNA] = 100 (b) and 200 μM (c), scan rate was 100 mV s^{-1}.

slower mass transfer of complexes bound to DNA fragments [54] lead to a decrease in concentration of the unbound redox-active species in solution. The considerable decrease in voltammetric current and potential suggests the existence of intercalation mode of binding between complexes and CT DNA bases [31,55]. The decrease in peak current is much higher for **2** than for others, sug-

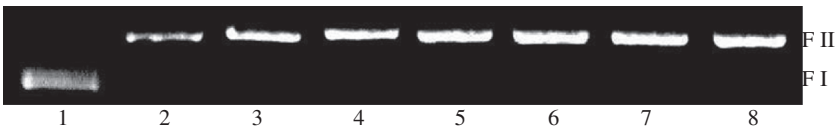

Fig. 7. Electrophoretogram showing the nuclease activity of complex **2** on pBR322 DNA (33.3 μM) in Tris–HCl/NaCl buffer (pH 7.2). Lane 1, DNA control; lanes 2–8, DNA + **2** (50, 100, 150, 200, 300, 400 and 500 μM, respectively).

gesting its stronger DNA binding, and follows the order of **2 > 1 > 3 > 4**. Thus, the observed results suggest that the complexes interact with DNA through an intercalative mode involving the stacking interaction between an aromatic ring and the base pairs of DNA. These results are in agreement with the above discussed techniques.

3.4. Cheminuclease activity

The chemi (or) chemical nuclease activity on plasmid DNA, explored by transition metal ions, has been of interest to researchers. The nuclease activity of complexes **1**–**4** have been studied using supercoiled (SC) pBR322 DNA (33.3 μM) in Tris–HCl/NaCl buffer at 37 °C by hydrolytic and oxidative pathway. This can be achieved by monitoring the transition from the covalently closed circular supercoiled form to the open circular relaxed form and linear form by gel electrophoresis of the plasmid. In both of the nuclease reactions, the control experiments do not show any considerable DNA cleavage.

The migration of DNA in gel electrophoresis works under the influence of electric potential. DNA is negatively charged species, and when it is placed under electric field, it will migrate towards anode and this migration depends on the DNA size, electric field, gel density and the nature of buffer. When circular plasmid DNA is run in horizontal using electrophoresis, relatively fast migration will be observed for the supercoiled form (Form I). If scission occurs, the supercoiled form will relax to generate a slower-moving open circular form (Form II), and if both strands are cleaved, a linear form (Form III) that migrates between Form I and Form II will be generated.

3.4.1. Hydrolytic cleavage

Transition metal complexes are the primary criteria for catalyzing hydrolytic cleavage of DNA, i.e., coordination and electrostatic interaction of the phosphate moiety of DNA to the metal(II) center of complex, its DNA cleaving ability has been investigated with various concentrations of complex. In general, the zinc(II) complexes cleave DNA by the hydrolytic pathway [56]. The nuclease activity of complexes **1**–**4** was observed in the absence of external agent and the increasing intensity of NC form was found with the increase in concentration of complexes (50–500 μM) without formation of LC form of DNA. Complexes **2** and **1** show prominent cleavage to give nicked circular (NC) form (~75%), while complexes **3** and **4** shows the activity lower than the expected efficiency (~30%). The electrophoretogram for **2** is shown in Fig. 7.

The presence of more aromatic moiety and hard Lewis acid properties of complexes could play a vital role in the DNA cleavage process by hydrolytic pathway [57]. Based on our results and literature [18,58], the following interaction was concluded between metal ion and phosphate moiety of DNA. The zinc(II) ion may recognize and bind with the phospho-diester bond of DNA through the coordinate linkage and/or electrostatic interaction, and the metal ion activate the central phosphorus atom of DNA, resulting in the formation of five coordinated phosphorus intermediate. Then, the activated phosphorus atom is attacked nucleophilically by the metal ion due to their Lewis acidity *via* charge neutralization, and finally one of the P—O ester bond of the nucleic acid is cleaved (Scheme 2). The obtained cheminuclease activity of complexes **1**–**4** by hydrolytic pathway varies as **2** > **1** > **3** > **4**.

3.4.2. Oxidative cleavage

The degradation of pBR322 DNA is also dependent on co-oxidant used. The cleavage of plasmid DNA induced by complexes **1**–**4** was investigated and clarified in the presence of H_2O_2 as a co-oxidant. Control experiments with DNA alone and DNA + H_2O_2 were also carried out and did not show any significant cleavage. All complexes induced degradation of the supercoiled Form I to yield nicked Form II. At 100 μM concentration, all complexes con-

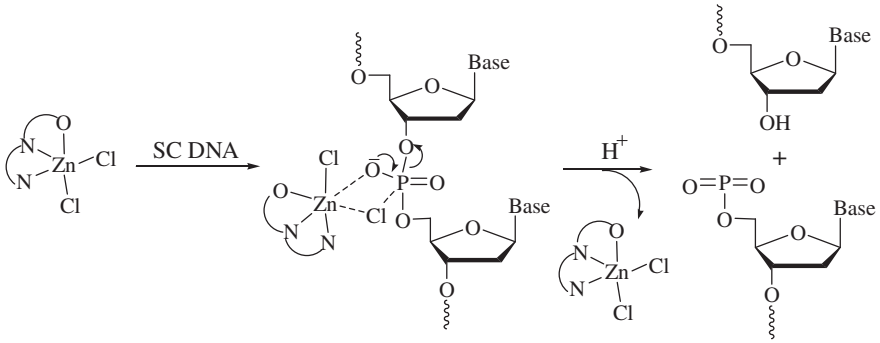

Scheme 2. A proposed hydrolytic cleavage mechanism of plasmid DNA.

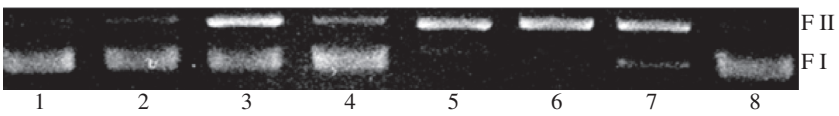

Fig. 8. Electrophoretogram showing the nuclease activity of complexes **1** and **2** on pBR322 DNA (33.3 μM) in the presence of H_2O_2 (40 μM) and DMSO (0.2 mM) in Tris–HCl/NaCl buffer (pH 7.2). Lane 1, DNA control; lanes 2/5, DNA + **1**/**2** (100 μM); lanes 3/6, DNA + **1**/**2** (100 μM) + H_2O_2; lanes 4/7, DNA + **1**/**2** (100 μM) + H_2O_2 + DMSO; lane 8, DNA + H_2O_2.

vert SC DNA into NC form revealing that these complexes behave as chemical nucleases in the presence of co-oxidant (Fig. 8).

The mechanism was proposed for oxidative cleavage of DNA by complexes as follows: The interaction of complexes of electrochemically active ligands with DNA in the presence of a co-oxidant is believed to produce different oxygen intermediates, depending on the specific complex and conditions. A non-diffusible metal-peroxo intermediate has been invoked in some cleavage reactions while in others, Fenton-like chemistry, which invokes release of freely diffusible hydroxyl ($OH^{\cdot}$) or hydroperoxyl ($HO_2^{\cdot}$) radical, has been assumed. The role of metal in the presence of H_2O_2 may generate reactive hydroxyl/hydroperoxyl radical that can damage the deoxyribose ring (C3′), or alternatively a metal-peroxo species may participate directly in the oxidation of the deoxyribose ring.

To apprehend the reactive oxygen species (ROS), standard scavengers of reactive oxygen intermediates were included in the electrophoresis studies. The cleavage of DNA mediated by complexes was diminished significantly in the presence of DMSO as hydroxyl radical scavenger, which conclusively shows the involvement of the hydroxyl radical as an intermediate in the DNA scission process. In addition, the coordination environment of the central metal ions and geometry of the complexes not only governs the DNA binding but also determine the nucleolytic action. Therefore, the difference in the nuclease activity of complexes may be attributed to their proximity to DNA binding. The cheminuclease activity of redox mediated or photo activated metal complexes is an important element in the characterization of DNA recognition of transition metal complexes.

4. Conclusions

In our present study, the principal findings and conclusions are as follows: The Schiff base ligands (HL^{1-4}) and its mononuclear zinc(II) complexes (**1**–**4**) were synthesized and characterized. Single crystal XRD analysis revealed that complex **4** exhibits distorted trigonal–bipyramidal geometry around metal center, with five coordination sites occupied by a tridentate ligand and two chloride anions. Cyclic voltammograms of ligands and complexes exhibit similar reduction process as zinc(II) ion is electrochemically innocent. All complexes bind with CT DNA through intercalation. Interestingly, **2** and **1** are efficient in nuclease activity on plasmid DNA in the absence and presence of H_2O_2 as co-oxidant than complexes **3** and **4**. Mechanistic studies indicate the involvement of hydroxyl radical as ROS. The DNA binding and cheminuclease activity exhibit a similar trend while expressing their potentials which follows the order **2** > **1** ≫ **3** > **4**. The higher DNA interaction of complex **2** may be due to the hydrophobic nature of methyl (—CH_3) substituent. These results should be valuable in understanding the interaction of the mononuclear zinc(II) complexes with DNA as well as laying a foundation for the rational design of novel, powerful agents for probing and targeting nucleic acids.

Acknowledgements

AKR gratefully thanks University Grants Commission (UGC), New Delhi, for financial assistance through the Major Research Project Grant [F.No. 39-797/2010 SR]. CK thanks UGC, New Delhi, for providing financial assistance in the form of fellowship. The authors thank Dr. Sultan Ahamed Ismail, D.Sc., Former Head, Department of Biotechnology, The New College (Autonomous), for providing facilities to carry out cheminuclease activity.

Appendix A. Supplementary material

CCDC 904783 contains the supplementary crystallographic data for complex **4**. These data can be obtained free of charge *via* http://www.ccdc.cam.ac.uk/conts/retrieving.html, or from the Cambridge Crystallographic Data Centre, 12-Union Road, Cambridge CB2 1EZ, UK; fax: +44 1223 336 033; or e-mail: deposit@ccdc.cam.ac.uk.

Supplementary data associated with this article can be found, in the online version, at http://dx.doi.org/10.1016/j.molstruc.2014.01.026.

References

[1] B. Hippert (Ed.), Cisplatin, Chemistry and Biochemistry of a Heading Anticancer Drug, Wiley-VCH, Weinhein, 1999.
[2] T. Boulikas, M. Vougiouka, Oncol. Rep. 10 (2003) 1663–1682.
[3] J.A. Cowan, Curr. Opin. Chem. Biol. 5 (2001) 634–642.
[4] S. Mathur, S. Tabassum, Cent. Eur. J. Chem. 4 (2006) 502–522.
[5] Y.J. Park, J.-W. Park, C.-H. Jun, Acc. Chem. Res. 41 (2008) 222–234.
[6] H. Nishiyama, J.-I. Ito, Chem. Commun. 46 (2010) 203–212.
[7] Z.J. Wang, K.N. Clary, R.G. Bergman, K.N. Raymond, F.D. Toste, Nat. Chem. 5 (2013) 100–103.
[8] M. Roy, B. Pathak, A.K. Patra, E.D. Jemmis, M. Nethaji, A.R. Chakravarty, Inorg. Chem. 46 (2007) 11122–11132.
[9] N. Shahabadi, S. Kashanian, F. Darabi, Eur. J. Med. Chem. 45 (2010) 4239–4245.
[10] R.J.P. Williams, in: C.F. Mills (Ed.), Zinc in Human Biology, Springer-Verlag, Berlin, Germany, 1989.
[11] H. Vahrenkamp, Dalton Trans. 42 (2007) 4751–4759.
[12] H. Steinhagen, G. Helmchen, Angew. Chem. 108 (1996) 2489–2492.
[13] Z.H. Chohan, M. Arif, M. Sarfraz, Appl. Organomet. Chem. 21 (2007) 294–302.
[14] Q. Huang, Z. Pan, P. Wang, Z. Chen, X. Zhang, H. Xu, Bioorg. Med. Chem. Lett. 16 (2006) 3030–3033.
[15] A. Guha, T. Chattopadhyay, N.D. Paul, M. Mukherjee, S. Goswami, T.K. Mondal, E. Zangrando, D. Das, Inorg. Chem. 51 (2012) 8750–8759.
[16] A. Guha, K.S. Banu, S. Das, T. Chattopadhyay, R. Sanyal, E. Zangrando, D. Das, Polyhedron 52 (2013) 669–678.
[17] N. Raman, K. Pothiraj, T. Baskaran, J. Mol. Struct. 1000 (2011) 135–144.
[18] S. Anbu, S. Kamalraj, B. Varghese, J. Muthumary, M. Kandaswamy, Inorg. Chem. 51 (2012) 5580–5592.
[19] A.-N.M.A. Alaghaz, B.A. El-Sayed, A.A. El-Henawy, R.A.A. Ammar, J. Mol. Struct. 1035 (2013) 83–93.
[20] J.C. Duff, J. Chem. Soc. (1941) 547–550.
[21] D.D. Perrin, W.L.F. Armarego, Purification of Laboratory Chemicals, third ed., Pergamon Press, 1988.
[22] L. Shi, H.-M. Ge, S.-H. Tan, H.-Q. Li, Y.-C. Song, H.-L. Zhu, R.-X. Tan, Eur. J. Med. Chem. 42 (2007) 558–564.
[23] A. Onder, M. Turkyilmaz, Y. Baran, Inorg. Chim. Acta 391 (2012) 28–35.
[24] Bruker-Nonius, APEX-II and SAINT-plus (Version 7.06a), Bruker AXS Inc., Madison, Wisconsin, USA, 2004.
[25] A. Altomare, G. Cascarano, C. Giacovazzo, A. Guagliardi, J. Appl. Crystallogr. 26 (1993) 343–350.
[26] G.M. Sheldrick, Acta Crystallogr. Sec. A 64 (2008) 112–122.
[27] L.J. Farrugia, J. Appl. Crystallogr. 30 (1997) 565.
[28] C.F. Macrae, P.R. Edgington, P. McCabe, E. Pidcock, G.P. Shields, R. Taylor, M. Towler, J. van de Streek, J. Appl. Crystallogr. 39 (2006) 453–457.
[29] J. Marmur, J. Mol. Biol. 3 (1961) 208–218.
[30] R. Reichmann, S.A. Rice, C.A. Thomas, P. Doty, J. Am. Chem. Soc. 76 (1954) 3047–3053.
[31] M.T. Carter, M. Rodriguez, A.J. Bard, J. Am. Chem. Soc. 111 (1989) 8901–8911.
[32] S.R. Smith, G.A. Neyhart, W.A. Karlsbeck, H.H. Thorp, New J. Chem. 18 (1994) 397–406.
[33] A.E. Friedman, J.C. Chambron, J.P. Sauvage, N.J. Turro, J.K. Barton, J. Am. Chem. Soc. 112 (1990) 4960–4962.
[34] G. Cohen, H. Eisenberg, Biopolymers 8 (1969) 45–55.
[35] S. Satyanarayana, J.C. Dabrowiak, J.B. Chaires, Biochemistry 31 (1992) 9319–9324.
[36] S. Mahadevan, M. Palaniandavar, Bioconjugate Chem. 7 (1996) 138–143.
[37] A. Pui, I. Berdan, I.M. Badarau, A. Gref, M.P. Fauvet, Inorg. Chim. Acta 320 (2001) 167–171.
[38] A. Ray, G.M. Rosair, R. Kadam, S. Mitra, Polyhedron 28 (2009) 796–806.
[39] N.B. Colthrup, L.H. Daly, S.E. Wiberley, Introduction to Infrared and Raman Spectroscopy, third ed., Academic Press Inc., San Diego, CA, 1990. pp. 1–73.
[40] M. Thirumavalavan, P. Akilan, M. Kandaswamy, K. Chinnakali, G. Senthil Kumar, H.K. Fun, Inorg. Chem. 42 (2003) 3308–3317.
[41] A.W. Addison, T.N. Rao, J. Reedijk, J. van Rijn, G.C. Verschoor, J. Chem. Soc., Dalton Trans. (1984) 1349–1356.
[42] P.K. Dhara, S. Pramanik, T.H. Lu, M.G.B. Drew, P. Chattopadhyay, Polyhedron 23 (2004) 2457–2464.
[43] T. Weyhermüller, R. Wagner, P. Chaudhuri, Eur. J. Inorg. Chem. 2011 (2011) 2547–2557.
[44] G.R. Desiraju, T. Steiner, The Weak Hydrogen Bond in Structural Chemistry and Biology, Oxford University Press, New York, 1999.

[45] H.P. Klug, L.E. Alexander, X-ray Diffraction Procedures for Polycrystalline and Amorphous Materials, second ed., Wiley, New York, 1974.
[46] S. Ramakrishnan, V. Rajendiran, M. Palaniandavar, V.S. Periasamy, B.S. Srinag, H. Krishnamurthy, M.A. Akbarsha, Inorg. Chem. 48 (2009) 1309–1322.
[47] G. Dougherty, W.J. Pigram, Crit. Rev. Biochem. 12 (1982) 103–132.
[48] S.A. Bejune, A.H. Shelton, D.R. McMillin, Inorg. Chem. 42 (2003) 8465–8475.
[49] D.S. Raja, N.S.P. Bhuvanesh, K. Natarajan, Eur. J. Med. Chem. 46 (2011) 4584–4594.
[50] M. Cory, D.D. Mckee, J. Kagan, D.W. Henry, J.A. Miller, J. Am. Chem. Soc. 107 (1985) 2528–2536.
[51] L. Jin, P. Yang, J. Inorg. Biochem. 68 (1997) 79–83.
[52] E.J. Gabbay, R.E. Scofield, C.S. Baxter, J. Am. Chem. Soc. 95 (1973) 7850–7857.
[53] H.-L. Chen, H.-Q. Liu, B.-C. Tzeng, Y.-S. You, S.-M. Peng, M. Yang, C.-M. Che, Inorg. Chem. 41 (2002) 3161–3171.
[54] D.H. Johnston, C.-C. Cheng, K.J. Campbell, H.H. Thorp, Inorg. Chem. 33 (1994) 6388–6390.
[55] C. Tolia, A.N. Papadopoulos, C.P. Raptopoulou, V. Psycharis, C. Garino, L. Salassa, G. Psomas, J. Inorg. Biochem. 123 (2013) 53–65.
[56] J. Tan, B. Wang, L. Zhu, Bioorg. Med. Chem. Lett. 17 (2007) 1197–1199.
[57] D. Desbouis, I.P. Troitsky, M.J. Belousoff, L. Spiccia, B. Graham, Coord. Chem. Rev. 256 (2012) 897–937.
[58] Q. Wang, H. Lonnberg, J. Am. Chem. Soc. 128 (2006) 10716–10728.